JOURNAL OF MATERIALS SCIENCE 29 (1994) 4415–4419

# Ultrasonic evaluation of elastic parameters of sintered powder compacts

A. K. MAITRA, K. K. PHANI
*Central Glass and Ceramic Research Institute, Calcutta 700032, India*

The variation of elastic moduli, $M$, of sintered powder compacts with porosity, $p$, has been analysed in terms of an equation $M = M_0 (1-p)^n$, where $M_0$ is the elastic modulus of non-porous material and $n$ is a constant. The variation of ultrasonic velocities has also been described in terms of a similar equation derived from the relations given by physical acoustics theory. It has been shown that the parameter $n$ is related to a stress concentration factor around pores in the material and is dependent on pore geometry and its orientation in the material. The observed variation in moduli and velocities with porosity has been compared with the theoretically predicted values based on self-consistent oblate spheroidal theory.

## 1. Introduction

Ultrasonic characterization of sintered powder metal parts and ceramics has long been of high interest and a number of such studies has been reported in the literature [1–4]. These studies usually involve measurements of ultrasonic velocities in materials and evaluation of the elastic properties. Because ultrasonic velocity is a relatively simple measurement that requires the material specimen to have one pair of sides flat and parallel, it provides an attractive method for non-destructive evaluation of material properties at different stages of fabrication as a means of quality control of the final product. In a review [5], Roth *et al.* have analysed the possible potential of this method in estimating the porosity fraction in polycrystalline ceramic and metallic materials and concluded that a relation of the type

$$V = V_0 (1 - p) \quad (1)$$

describes the variation of ultrasonic velocity, $V$, with porosity, $p$, best. $V_0$ is the velocity of non-porous material. On the other hand, in other studies [3, 4], it has been shown that relations of the type

$$M = M_0 \exp(-ap) \quad (2)$$

and

$$M = M_0 \exp[-(ap + bp^2)] \quad (3)$$

provide the best fit to the experimental data on elastic modulus. In these relations, $M$ is the Young's or shear modulus ($E$ or $G$); $a$ and $b$ are empirical constants. The subscript 0 refers to zero porosity values. According to physical acoustics theory, elastic moduli and ultrasonic velocities are related by

$$V_l = \left[\frac{E(1-\nu)}{\rho(1+\nu)(1-2\nu)}\right]^{1/2} \quad (4)$$

$$V_S = (G/\rho)^{1/2} \quad (5)$$

where $V_l$ and $V_S$ are longitudinal and transverse ultrasonic velocities, respectively, $\nu$ is Poisson's ratio, and $\rho$ is the density. Thus if Equation 1 is used to describe the velocity–porosity relation, Equations 4 and 5 show that a third-degree polynomial should be used for moduli-porosity relation. Conversely, Equations 3, 4 and 5 dictate that an exponential relation should provide the best description of velocity–porosity data. Also, for sintered industrial clay ceramics, the values of $V_0$ obtained by Panakkal [4] by fitting experimental data to Equation 1, differed by as much as $\sim$ 30% from those calculated from zero-porosity moduli values which were obtained by fitting Equation 2 to empirical data. Thus, it is apparent that inconsistencies exist in the relations that have been used in analysing the ultrasonic data on sintered powder compacts. In this paper we address this issue, utilizing the data reported by Panakkal *et al.* [3] on sintered iron powder compacts.

Furthermore, previous studies [3, 4] have compared the experimental data with the theoretical values based on elastic theory [6–8] and the self-consistent scattering theory [9]. For sintered clay ceramics [4], both the theories grossly overestimated the value over the entire range of porosity under investigation. For sintered iron powder compacts [3], scattering theory provided better agreement than the elastic theory but for both the theories deviations from the theoretical values increased as pore volume increased. This was attributed to non-sphericity of the starting powder, the irregular stacking pattern of the initial powders compared to the simple cubic pattern assumed in the theory, and the non-sphericity of pores at higher porosities. This issue is also analysed in this paper, based on the self-consistent oblate spheroidal theory.

## 2. Data analysis

The data used in this analysis are those reported by Panakkal *et al.* [3] for hot isostatically pressed and

0022–2461 

sintered iron compacts. They measured the ultrasonic velocity (longitudinal and transverse) and evaluated the elastic moduli and Poisson's ratio of compacts as a function of porosity (up to 21.6%). They analysed the moduli–porosity data in terms of Equations 2 and 3 and the equation given by Hashin [10]. Equation 3 provided best fit to their data, yielding zero-porosity Young's and shear moduli values as 207 and 80 GPa, respectively. These values agree well with the respective Young's and shear moduli values of 212 and 82 GPa of electrolytic iron. They did not analyse the variation of velocity with porosity.

Equation 3 is an extension of Equation 2 proposed by Wang [8]. He has shown that Equation 2 holds good only up to a porosity range of 20%, and the modification proposed by him extends its validity up to a porosity range of 30%. However, both these equations suffer from the drawback that they do not satisfy the boundary condition of the physical phenomenon it represents, i.e. $M = 0$ at $p \leqslant 1$. Because of this, use of these equations to evaluate elastic moduli of theoretically dense material by extrapolation from fitted experimental data has sometimes resulted in large discrepancies between the extrapolated and observed values [11, 12]. Soroka and Sereda [12] have studied the porosity dependence of gypsum over two different porosity ranges, $0.11 \leqslant p \leqslant 0.3$ and $0.49 \leqslant p \leqslant 0.70$, using Equation 2 and obtained values of $E_0$ differing by one order of magnitude. To resolve this problem, Phani [13] has shown that a relation of the form

$$M = M_0(1-p)^n \tag{6}$$

where $n$ is an empirical constant, can describe the data over the entire range of porosity. We use the same relation to analyse the data here.

Equation 6 was fitted to both Young's and shear moduli data by non-linear regression analysis following the method of Lewis [14]. The sum of squares, $Q$, was used as the measure of the goodness of the fit between the fitted equation and data

$$Q = 1 - \sum_{i=1}^{n} (M_i - \hat{M}_i)^2 \Big/ \sum_{i=1}^{n} (M_i - \bar{M}_i)^2 \tag{7}$$

where $\hat{M}_i$ is the value calculated from the fitted equation for appropriate $p$ value, $M_i$ and $\bar{M}_i$ are the measured values and mean value, respectively. For good fit, $Q \geqslant 0.95$, for $Q < 0.9$ the fit is poor. The equations that fit the data are

$$\text{Young's modulus, } E(\text{GPa}) = 216.2(1-p)^{3.131} \tag{8}$$

$$\text{shear modulus, } G(\text{GPa}) = 83.4(1-p)^{2.877} \tag{9}$$

with $Q$ values of 0.953 and 0.952 for Young's and shear moduli, respectively, indicating a good agreement between the fitted equations and the data. The zero porosity moduli values are also in close agreement with the values of 212 and 82 GPa for Young's and shear moduli of electrolytic iron, respectively. The fitted equations, together with the data, are shown in Fig. 1.

If we combine Equations 4 and 5 with Equation 6 and use the relation

$$\rho = \rho_0(1-p) \tag{10}$$

where $\rho_0$ is the theoretical density, ultrasonic velocity–porosity relations are given by

$$V_1 = V_{01}(1-p)^{(n-1)/2} = V_{01}(1-p)^m \tag{11}$$

$$V_S = V_{0S}(1-p)^{(n_1-1)/2} = V_B(1-p)^{m_1} \tag{12}$$

where $m = (n-1)/2$, $m_1 = (n_1 - 1)/2$ and

$$V_{01} = \left[\frac{E_0(1-\nu_0)}{\rho_0(1+\nu_0)(1+2\nu_0)}\right]^{1/2} \tag{13}$$

$$V_{0S} = (G_0/\rho_0)^{1/2} \tag{14}$$

It may be noted that in deriving Equation 11, we have neglected the variation of Poisson's ratio, $\nu$, with porosity.

Using $\nu_0 = 0.297$ and $\rho_0 = 7.8\ \text{g cm}^{-3}$ and substituting values of $E_0$, $G_0$, $n$ and $n_1$ from Equations 8 and 9, in Equations 11–14 we obtain

$$V_L(\text{mm}\,\mu\text{s}^{-1}) = 6.14(1-p)^{1.066} \tag{15}$$

$$V_S(\text{mm}\,\mu\text{s}^{-1}) = 3.27(1-p)^{0.939} \tag{16}$$

These equations are plotted in Fig. 2, showing fair agreement with the data. Also, the zero porosity longitudinal and shear velocity values of 6.14 and 3.27 $\text{mm}\,\mu\text{s}^{-1}$, agree well with the values of 6.02 and 3.24 $\text{mm}\,\mu\text{s}^{-1}$, calculated from the moduli values of electrolytic iron, respectively.

Conversely, if we start with the relations given by Equations 11 and 12 and fit to the velocity pore fraction data, it yields relations

$$V_1(\text{mm}\,\mu\text{s}^{-1}) = 6.07(1-p)^{1.459} \tag{17}$$

$$V_S(\text{mm}\,\mu\text{s}^{-1}) = 3.29(1-p)^{1.102} \tag{18}$$

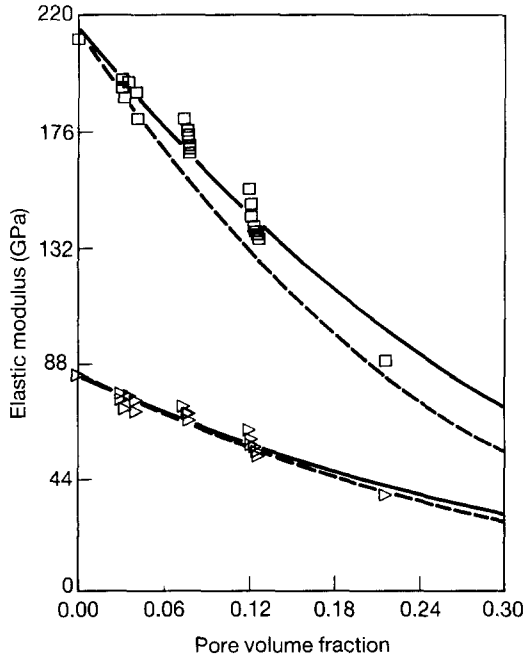


*Figure 1* Variation of elastic moduli with pore volume fraction. (——) Equations 8 and 9, (···) derived equations (19) and (20). (⊡) Young's, (▷) shear moduli.

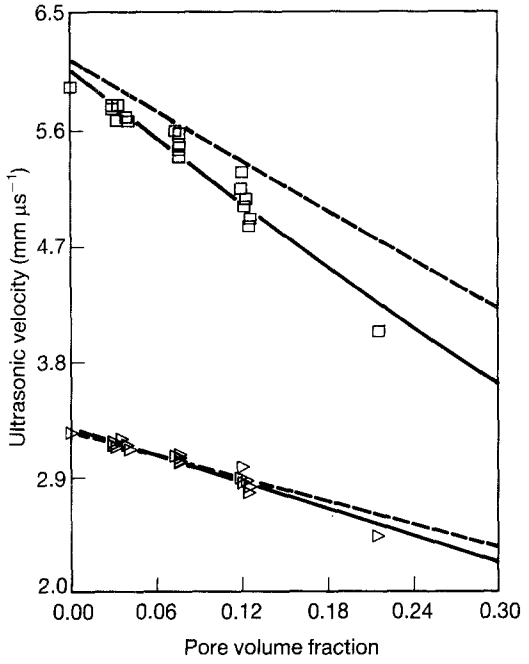


*Figure 2* Variation of ultrasonic velocity with pore volume fraction. (——) Equations 17 and 18, (···) derived equations 15 and 16. (⊡) longitudinal, (▷) Shear moduli.

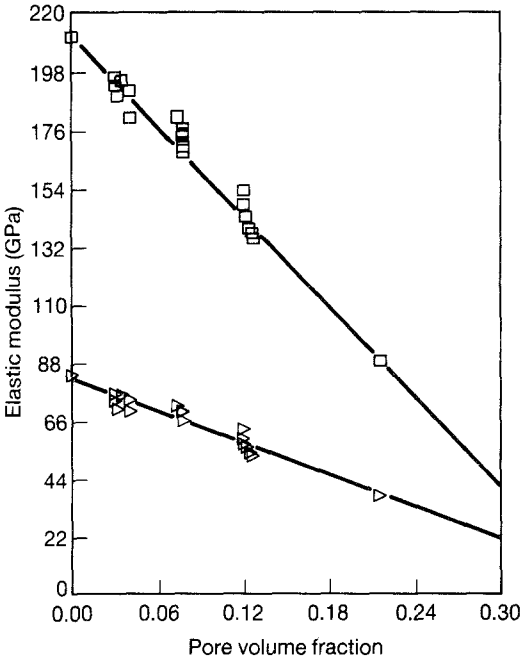


*Figure 3* Elastic moduli against pore volume fraction. (——) Theoretical curves for $\alpha = 0.273$. (⊡) Young's; (▷) shear moduli.

with $Q$ values of 0.940 and 0.943 for longitudinal transverse velocity, respectively. These equations are also plotted in Fig. 2, showing good agreement with the data. Equations 4, 5 and 10 can again be used to derive the moduli–porosity relation from the fitted Equations 17 and 18. This gives the relations

$$E(\text{GPa}) = 215.64(1-p)^{3.918} \quad (19)$$

$$G(\text{GPa}) = 84.65(1-p)^{3.203} \quad (20)$$

These equations are again plotted in Fig. 1 showing fair agreement with the data. Thus, Equations 6 and 11 not only explain the variation of elastic moduli and ultrasonic velocity with pore volume fraction but are also consistent with the relations derived from physical acoustic theory.

The variations of Poisson's ratio with the pore volume fraction can be derived from Equations 8 and 9 using the relation

$$\nu = E/2G - 1 \quad (21a)$$

giving

$$\nu = 1.297(1-p)^{0.254} - 1 \quad (21b)$$

Expanding the first term on the right-hand side binomially and neglecting terms of order higher than $p$, the equation reduces to

$$\nu = 0.297(1 - 1.11p) \quad (22)$$

Equation 22, together with the measured values of Poisson's ratio, are presented in Fig. 4. The $Q$ value works out to be 0.519, showing poor agreement between the predicted equation and the data. This is to be expected, considering the fact Poisson's ratio is a small quantity dependent on the differences of the other elastic properties and is very sensitive to errors in them.

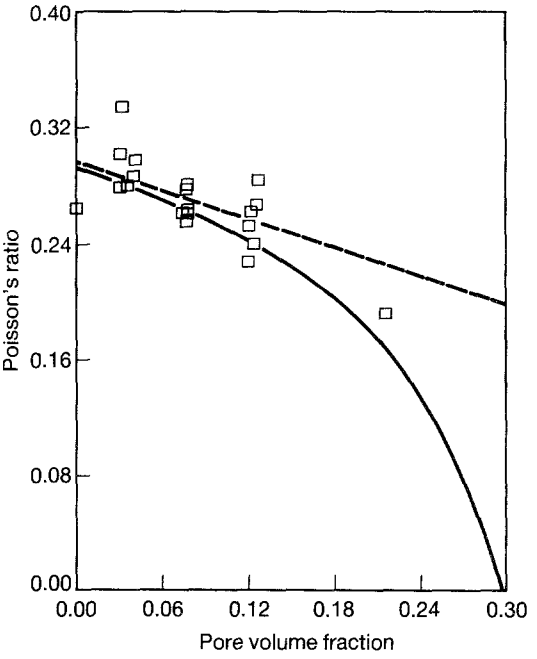


*Figure 4* Variation of Poisson's ratio with pore volume fraction. (···) Equation 22, (——) theoretical curve for $\alpha = 0.273$.

## 3. Theoretical predictions

Panakkal *et al.* [3] compared the elastic moduli data with the theoretically calculated values based on elasticity and scattering theories [6–9]. Although the variation of the moduli as a function of porosity was in good agreement with the theory (the slopes), the agreement between the theoretical values and data was not good. Of the two theories, the behaviour predicted by the self-consistent scattering theory was close to the experimental observation compared to elasticity theory. This was mainly attributed to the non-spherical nature of pores which was evident from the photomicrographs given in their paper. To the

best of our knowledge, the only theory that has been used to account for the effect of non-sphericity of pores on elastic moduli is one based on the self-consistent oblate spheroidal theory [15]. Dean [15] used the self-consistent scheme (SCS) given by Wu [16] and, considering the pores to be oblate spheroids, fitted both the measured Young's modulus and shear modulus versus porosity data to theory using spheroid aspect ratio as the only variable.

For porous material, Wu's [16] SCS theory gives the effective bulk modulus, $K$, and shear modulus, $G$, as

$$K = K_0[1 - pP_0(\alpha, R)] \quad (23)$$

$$G = G_0[1 - pQ_0(\alpha, R)] \quad (24)$$

where $P_0$ and $Q_0$ are functions of the aspect ratio, $\alpha$, of the spheroids, and $R$ is defined as

$$R = 3G/(3K + 4G) \quad (25)$$

Spheroids are characterized by the ratio of the minor axis to major axis, the aspect ratio, $\alpha$. Spheroids for which $\alpha = 1$ are spheres and as $\alpha$ approaches zero, oblate spheroids become disc-shaped and prolate spheroids become needle-shaped. Equations 23 and 24 were fitted to the data following the method given by Dean [15]. The values $E_0 = 212.0$ GPa and $G_0 = 82.0$ GPa for electrolytic iron were used in the theoretical calculation. The experimental data, together with the SCS oblate spheroidal theory with $\alpha = 0.273$ (solid lines), are shown in Fig. 3 for both Young's modulus and shear modulus. Agreement of experimental data with the theory was again worked out in terms of the sum of squares $Q$. It yielded values of 0.965 and 0.935 for Young's and shear moduli, respectively, showing excellent agreement between theory and experiment.

As pointed out by Dean [15], a more sensitive test of the power of this theory is a comparison between the theoretical results for Poisson's ratio and the values of this isotropic elastic constant calculated from the measured values of $E$ and $G$. This comparison is shown in Fig. 4. The closeness of the calculated points to the theoretical curves is quite good.

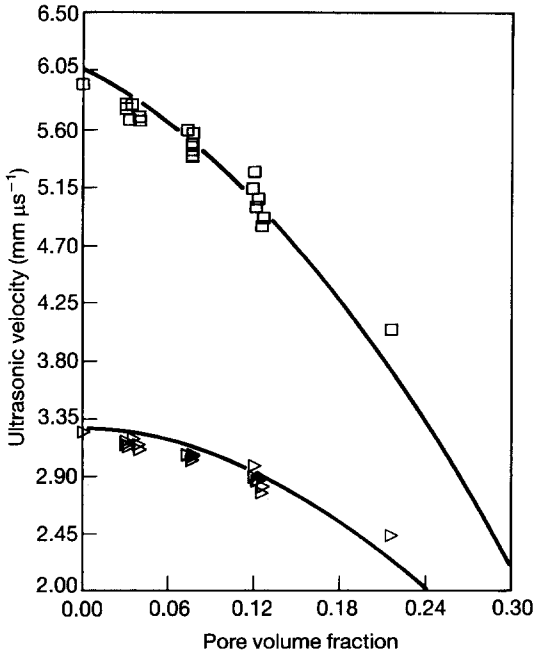


*Figure 5* Ultrasonic velocity against pore volume fraction. (——) Theoretical curves for $\alpha = 0.273$. (⊡) Longitudinal, (▷) shear moduli.

Theoretical velocity values were also computed from Equations 23 and 24 using relations

$$V_l = [(K + 4/3\,G)/\rho]^{1/2} \quad (26)$$

$$V_s = (G/\rho)^{1/2} \quad (27)$$

These values for an oblate spheroid of aspect ratio $\alpha = 0.273$, together with the experimental data, are shown in Fig. 5. Fig. 5 speaks for itself in terms of comparison between experiment and SCS oblate spheroidal theory.

It may be mentioned here that spheroids of a single aspect ratio, $\alpha = 0.273$, fit the data of a batch of sintered materials with individual members having large ranges of porosities. It is highly unlikely that all the pores will have the same aspect ratio. Thus, as shown by Dean [15], $\alpha$ should be considered as an "effective" aspect ratio which approximates the effect of a spectrum of aspect ratios.

## 4. Discussion

For $p \leqslant 0.10$, Equation 6 can be approximated to

$$E = E_0(1 - np) \quad (28)$$

Rossi [17] has shown, in that case, $n$ is given by the stress concentration factor about pores in the material. He has also calculated the values of stress concentration factor as a function of aspect ratio of spheroids for both oriented and random orientation of pores in the material. For spherical pores, the stress concentration factor is solely a function of the Poisson's ratio of the material and its value is equal to 2 for a Poisson's ratio of 0.2. For orientated oblate spheroidal pores the value can be approximated (for $\nu = 0.2$) by [17]

$$n = \frac{5}{4\alpha} + \frac{3}{4} \quad (29)$$

If we substitute the value of $n$ from Equation 8, it gives (the small variation due to difference in Poisson's ratio is neglected) $\alpha = 0.525$, which is almost twice the value obtained from SCS oblate spheroidal theory. On the other hand, if the pores are considered to be randomly oriented, the value of $\alpha$ becomes equal to 0.283 (refer to Fig. 8 in [17]). This value is in good agreement with $\alpha = 0.273$ obtained from SCS oblate spheroidal theory. Thus the exponent $n$ can be associated with stress concentration about pores in the material and its value will be dependent on pore geometry and its orientation.

For spherical pores, the value of $n = 2$. As $\alpha$ decreases the value of $n$ increases, and for random orientation of pores, $n = 4$ for $\alpha \simeq 0.18$ (Fig. 8 in [17]). Fig. 6 shows the relative moduli of 12 polycrystalline materials reported in the literature. These values lie in the range $(1 - p)^3$ to $(1 - p)^4$ with corresponding aspect ratio of randomly oriented oblate spheroids varying from 0.3–0.18. Equations 11 and 12 give the

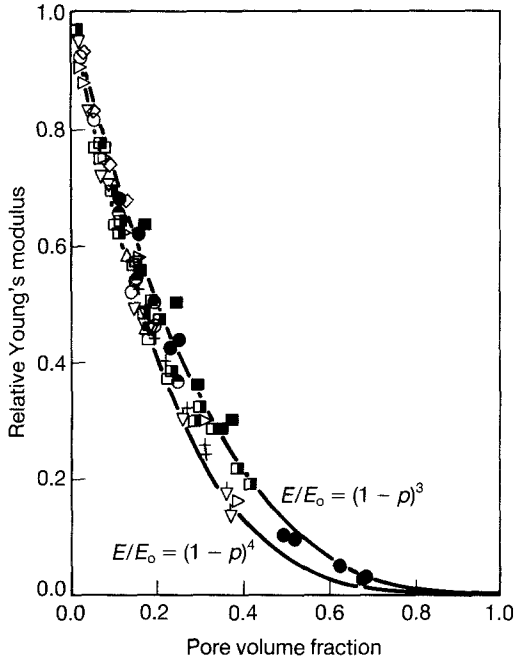


*Figure 6* Relative Young's modulus versus porosity for polycrystalline oxides. (●) Gypsum, (◨) $\alpha - Al_2O_3$, (▽) $\beta$-$Al_2O_3$, (▷) $MgAl_2O_4$, (◇) multite, ( + ) graphite, (□) $ZrO_2$, (▽) $CoAl_2O_4$, (△) CoO, (■) $Si_3N_4$, (◒) $HfO_2$, (○) SiC.

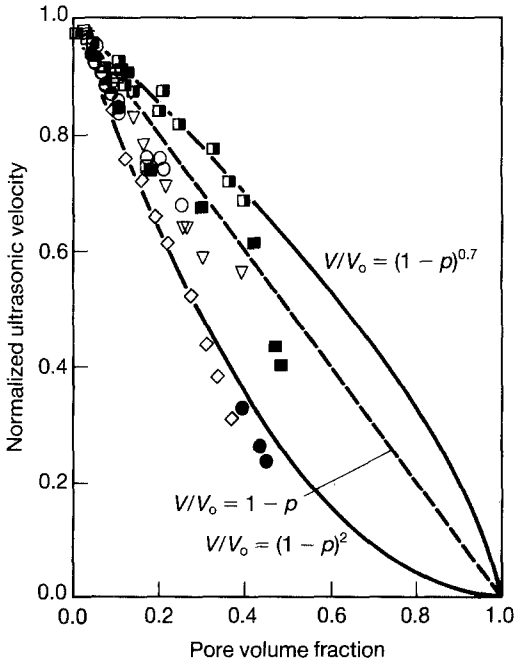


*Figure 7* Normalized longitudinal ultrasonic velocity versus porosity for polycrystalline materials. (●) MgO, (◨) $Al_2O_3$, (◇) porcelain, (□) SiC, (△) $Si_3N_4$, (■) tungsten, (◒) $UO_2$, (○) $YBa_2Cu_3O_{(7-x)}$.

corresponding velocity relations as

$$V = V_0(1 - p) \tag{30}$$

to

$$V = V_0(1 - p)^{1.5} \tag{31}$$

Fig. 7 shows the normalized velocity data of eight polycrystalline materials analysed by Roth *et al.* [5]. Velocity values were normalized using the zero porosity velocity values given by Roth *et al.* [5]. They lie in the range $(1 - p)^{0.7}$ to $(1 - p)^2$ and corresponding values of $n$ are in the range 2.4–5. The dotted line shown in the figure corresponds to the linear Equation 30 which has been used by Roth *et al.* [5] in their review. On the other hand, if Equation 31 is approximated by a linear one for porosity values greater than 0.20, it will tend to overestimate or underestimate the zero porosity value depending on the range of porosity over which the data are being fitted.

Finally, Panakkal *et al.* [3] have suggested a linear relationship between moduli and velocity for lower pore volumes. This is also confirmed from the present study, because for lower pore volumes, Equations 6, 11 and 12 can be approximated by linear equations, and the elimination of the variable, $p$, between them yields the desired linear relation.

## 5. Conclusion

Elastic moduli of sintered iron compacts as a function of porosity have been analysed in terms of an equation $M = M_0(1 - p)^n$. The constant $n$ is the stress concentration factor due to the presence of pores in the material and is dependent on pore geometry and its orientation in the material. Variation of ultrasonic velocity with porosity is also described by a similar relation which is consistent with the theories of physical acoustics.

Theoretical predictions based on the self-consistent oblate spheroidal theory explained well the observed variation of the elastic parameters and ultrasonic velocities. Data analysis indicates that ultrasonic velocity may be used to evaluate the elastic moduli of porous material.

## Acknowledgement

The authors thank Dr B. K. Sarkar, Director of the Institute for his permission to publish this paper.

## References

1. E. P. PAPADAKIS and B. W. PATERSEN, *Mater. Eval.* **37** (1979) 76.
2. R. M. ARONS and D. S. KUPPERMAN, *ibid.* **40** (1982) 1076.
3. J. P. PANAKKAL, H. WILLEMS and W. ARNOLD, *J. Mater. Sci.* **25** (1990) 1397.
4. J. P. PANAKKAL, *Br. J. NDT* **34** (1992) 529.
5. D. J. ROTH, D. B. STANG, S. M. SWICKARD and M. R. DEGUIRE, NASA Technical Memorandum 102501, July 1990, p 3.
6. R. W. RICE, in "Treatise on Material Science and Technology", Vol. 11, edited by R. K. MacCrone (Academic Press, New York, 1977) p. 199.
7. G. ONDRACEK, *Z. Werkstofftech.* **9** (1978) 31.
8. J. C. WANG, *J. Mater. Sci.* **19** (1984) 809.
9. C. M. SAYERS and R. L. SMITH, *Ultrasonics* **19** (1982) 201.
10. Z. HASHIN, *J. Appl. Mech.* **29** (1962) 143.
11. D. P. H. HASSELMAN, *J. Am. Ceram. Soc.* **45** (1962) 452.
12. I. SOROKA and P. J. SEREDA, *ibid.* **51** (1968) 337.
13. K. K. PHANI, *Am. Ceram. Soc. Bull.* **65** (1986) 1584.
14. D. LEWIS III, *ibid.* **57** (1978) 434.
15. E. A. DEAN, *J. Am. Ceram. Soc.* **66** (1983) 847.
16. T. T. WU, *Int. J. Solids Struct.* **3** (1966) 1.
17. R. C. ROSSI, *J. Am. Ceram. Soc.* **51** (1968) 433.

*Received 16 November 1993*
*and accepted 21 March 1994*